

Enhanced near-field radiative heat transfer between borophene sheets on different substrates

Xiaoyang Han(韩小洋) and Chunzhen Fan(范春珍)†
Citation: Chin. Phys. B, 2024, 33 (**12**): 127802. DOI: 10.1088/1674-1056/ad84cd
Journal homepage: http://cpb.iphy.ac.cn; http://iopscience.iop.org/cpb

What follows is a list of articles you may be interested in

Near-field radiative heat transfer between nanoporous GaN films

Xiaozheng Han(韩晓政), Jihong Zhang(张纪红), Haotuo Liu(刘皓佗), Xiaohu Wu(吴小虎), and Huiwen Leng(冷惠文)
Chin. Phys. B, 2024, 33 (**4**): 047801. DOI: 10.1088/1674-1056/ad09a9

Temperature-dependent photoluminescence of lead-free cesium tin halide perovskite microplates

Jiayu Tan(谭佳雨), Yixuan Zhou(周译玄), De Lu(卢德), Xukun Feng(冯旭坤), Yuqi Liu(刘玉琪), Mengen Zhang(张蒙恩), Fangzhengyi Lu(卢方正一), Yuanyuan Huang(黄媛媛), and Xinlong Xu(徐新龙)
Chin. Phys. B, 2023, 32 (**11**): 117802. DOI: 10.1088/1674-1056/ad028e

Probing photocarrier dynamics of pressurized graphene using time-resolved terahertz spectroscopy

Yunfeng Wang(王云峰), Shujuan Xu(许淑娟), Jin Yang(杨金), and Fuhai Su(苏付海)
Chin. Phys. B, 2023, 32 (**6**): 067802. DOI: 10.1088/1674-1056/acc2b1

Atomic-scale insights of indium segregation and its suppression by GaAs insertion layer in InGaAs/AlGaAs multiple quantum wells

Shu-Fang Ma(马淑芳), Lei Li(李磊), Qing-Bo Kong(孔庆波), Yang Xu(徐阳), Qing-Ming Liu(刘青明), Shuai Zhang(张帅), Xi-Shu Zhang(张西数), Bin Han(韩斌), Bo-Cang Qiu(仇伯仓), Bing-She Xu(许并社), and Xiao-Dong Hao(郝晓东)
Chin. Phys. B, 2023, 32 (**3**): 037801. DOI: 10.1088/1674-1056/ac70b5

Effect of thickness of antimony selenide film on its photoelectric properties and microstructure

Xin-Li Liu(刘欣丽), Yue-Fei Weng(翁月飞), Ning Mao(毛宁), Pei-Qing Zhang(张培晴), Chang-Gui Lin(林常规), Xiang Shen(沈祥), Shi-Xun Dai(戴世勋), and Bao-An Song(宋宝安)
Chin. Phys. B, 2023, 32 (**2**): 027802. DOI: 10.1088/1674-1056/ac8724

Enhanced near-field radiative heat transfer between borophene sheets on different substrates

Xiaoyang Han(韩小洋) and Chunzhen Fan(范春珍)†

Key Laboratory of Materials Physics, Ministry of Education, School of Physics, Zhengzhou University, Zhengzhou 450001, *China*

(Received 29 July 2024; revised manuscript received 5 September 2024; accepted manuscript online 9 October 2024)

Near-field radiative heat transfer (NFRHT) has the potential to exceed the blackbody limit by several orders of magnitude, offering significant opportunities for energy harvesting. In this study, we have examined the NFRHT between two borophene sheets through the calculation of heat transfer coefficient (HTC). Due to the tunneling of evanescent waves, borophene sheet allows for enhanced heat flux and adjustable NFRHT by varying its electron density and electron relaxation time. Additionally, the near field coupling is further examined when the borophene is deposited on dielectric or lossy substrates. The maximum HTC is closely related to the real part of the dielectric substrate. As a case study, the HTCs on the lossy substrate of MoO_3, ZnSe, and SiC are calculated for comparisons. Our results indicate that MoO_3 is the optimal substrate to get the enhanced energy transfer coefficient. It results in a remarkable value of 1737 times higher than the blackbody limit owing to the enhanced photon tunneling probability. Thus, our study reveals the effect of substrate on the HTC between borophene sheets and provides a theoretical guidance for the design of near-field thermal radiation devices.

Keywords: near-field radiative heat transfer, borophene, lossy substrate, heat transfer coefficient

PACS: 78.20.–e, 71.36.+c, 78.20.Bh **DOI:** 10.1088/1674-1056/ad84cd

1. Introduction

When the separation between two objects is smaller than the characteristic wavelength of thermal radiation (~ 10 μm at 300 K), the coupling effect of evanescent modes becomes significant, causing radiative heat transfer to greatly exceed the conventional blackbody limit.[1–4] Since the pioneering work of Bold and van Hove,[5] NFRHT has been remarkably investigated both theoretically[6–10] and experimentally[11–15] over the past two decades. Initially, Hargreaves *et al.*[16] found an enhanced heat transport between the Gr–Gr inter planar with a distance of 1-μm pitch. Hu *et al.*[17] demonstrated the near-field heat flux between two quartz flat plates could surpass the blackbody limit at room temperature in 2008. Subsequent experiments were carried out at even smaller separations, and the obtained heat flux exceeds the blackbody limit by up to four orders of magnitude. Early studies on near-field thermal radiation mainly involved two-plate configuration, and then it extended to multi-plates,[18] tip–plate,[13] and tip–tip structures. Owing to its high heat flux, NFRHT holds tremendous potential for applications in energy harvesting systems,[19,20] thermal switchers,[21,22] and transistors.[23,24]

Recently, two-dimensional (2D) materials have attracted much attention due to their unique electronic and optical properties.[25–27] Graphene,[28–30] as the most representative 2D material, can excite surface plasmon polaritons[31] in the near-field regime thereby enhancing and tunable near-field thermal radiation can be achieved. Black phosphorus (BP)[32,33] also supports surface plasmons and it exhibits in-plane anisotropic optical and electrical properties, which has sparked numerous intriguing studies in near-field thermal radiation. Hexagonal boron nitride (hBN) is a natural hyperbolic material,[34,35] which supports hyperbolic modes with high wave vectors in these two Reststrahlen bands.[36] Its unique properties enable it to achieve near-field thermal radiation over a wide wavelength range like a blackbody. To date, numerous studies have been conducted to investigate how different substrates affect NFRHT between graphene sheets. Habibzadeh *et al.*[37] compared modulation ratios and near-field heat flow between graphene sheets on 41 different substrates and independent graphene sheets. Svetovoy *et al.*[38] analyzed the variation of near-field radiative heat transfer in graphene-covered dielectrics. Wang *et al.*[39] investigated near-field radiative heat transfer in metals with and without graphene layers, doped silicon and polar dielectrics. These studies have revealed the importance of substrates in the study of NFRHT. In 2015, Mannix *et al.* successfully synthesized borophene monolayers on Ag (111) substrates to include the metallic state.[40] In addition, borophene possesses an ultra-high electron density ($> 10^{15}$ cm^{-2}) and exhibits strong anisotropy and surface plasmon-polarized excitons. Prior investigations into the NFRHT between suspended borophene sheets with a separation of 10 nm have revealed that the heat flux can reach up to 1289 times the radiative heat flux of the blackbody limit ($q_{\rm bb}$) of 3.08 W·m^{-2} at a temperature difference of 200 K.[41] While the previous studies on NFRHT with borophene have focused on suspended sheets, it is imperative to consider the influence of substrate on their NFRHT.

In this work, we have explored the NFRHT between two

†Corresponding author. E-mail: chunzhen@zzu.edu.cn

© 2024 Chinese Physical Society and IOP Publishing Ltd

borophene sheets on dielectric or lossy substrates. The regulation of NFRHT can be effectively achieved with different electron density and relaxation time of borophene. A comprehensive analysis was conducted to elucidate the relationship between the real and imaginary components of the substrate and the consequent enhancement of HTC. As a case study, the HTCs of MoO_3, ZnSe, and SiC were calculated for comparisons with the inclusion of intrinsic loss, and the calculated energy transmission coefficient (ETC) as a function of angular frequency and wave vector is consistent with the numerical study. Owing to the anisotropic borophene, there was a marked disparity in the ETC along the x and y directions of the borophene. Finally, the influence of gap distance and temperature difference on NFRHT were finely discussed, the HTC tended to decrease linearly with a larger distance and increases gradually with a higher temperature difference.

2. Design and theory

The design of NFRHT between two borophene sheets with supporting substrates is illustrated in Fig. 1(a). The temperature of the emitter and receiver are denoted as T_1 and T_2, respectively. T_2 is the room temperature of 300 K. The gap distance is d, and the dielectric constant of the substrate is denoted as ε_s. An enlarged view of the crystal structure of borophene with hexagonal holes and triangular cavities is indicated in Fig. 1(b). The anisotropic optical conductivity of the monolayer borophene can be described by the semi-classical Drude model as follows:[42]

$$\sigma_{ll}(\omega) = \frac{\mathrm{i}e^2 n}{(\omega + \mathrm{i}/\tau)m_l}, \tag{1}$$

where l is the direction of optical axes along x or y, ω is the angular frequency, τ is the electron relaxation time, e is the electron charge, and n is the electron density of borophene. The effective electron mass m_l along the x direction and y direction are $m_x = 1.4m_0$, $m_y = 3.4m_0$,[43] and m_0 represents the rest mass of an electron. Figure 2 depicts the anisotropic conductivity of borophene in the x and y directions. The real part of the conductivity gets smaller as the angular frequency increases in Fig. 2(a). Meanwhile, figure 2(b) shows that the imaginary part of the conductivity initially increases and then decreases with a larger angular frequency. The anisotropic conductivity of borophene significantly influences its light–matter interactions, thereby altering the material's reflection, absorption, and transmission characteristics. This directional dependence directly impacts the propagation speed and mean free path of phonons, which in turn affects the heat transfer coefficients.

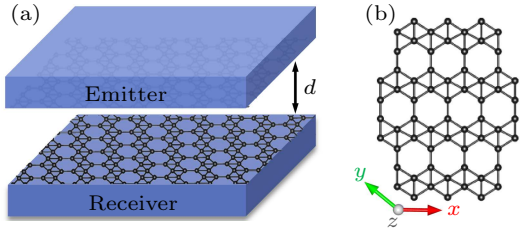


Fig. 1. (a) Schematic diagram of design of near-field heat transfer between borophene emitter and receiver, (b) illustration of the crystalline structure of borophene.

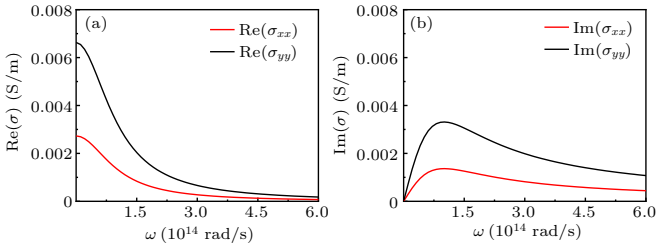


Fig. 2. (a) Real part and (b) imaginary part of the conductivity of borophene sheet with $\tau = 10$ fs and $n = 3.3 \times 10^{15}$ cm^{-2}.

To assess the near-field radiative heat transfer, we resort to the fluctuational electrodynamics with the dyadic Green's functions. It enables the calculation of HTC between borophene sheets as follows:[1,3]

$$\begin{aligned} q &= \int_0^\infty q(\omega)\,\mathrm{d}\omega \\ &= \frac{1}{4\pi^2}\int_0^\infty \mathrm{d}\omega \frac{\partial \Theta(\omega,T)}{\partial T} \sum_{j=\mathrm{s,p}} \int_0^\infty \xi_j(\omega,\beta)\beta\,\mathrm{d}\beta, \end{aligned} \tag{2}$$

where $q(\omega)$ denotes the spectral heat flux, it is a function of frequency. $\Theta(\omega,T) = \hbar\omega/(\mathrm{e}^{\hbar\omega/k_\mathrm{B}T} - 1)$ is the mean energy of a Planck oscillator, $\hbar$ is the Planck constant, β is the wave vector component. $\xi(\omega,\beta)$ is the energy transmission coefficient (ETC)

$$\xi_j(\omega,\beta) = \begin{cases} \dfrac{(1-|r_1^j|^2)(1-|r_2^j|^2)}{|1-r_1^j r_2^j \mathrm{e}^{2\mathrm{i}k_{z0}d}|^2}, & (\beta < k_0), \\ \dfrac{4\,\mathrm{Im}\,(r_1^j)\,\mathrm{Im}\,(r_2^j)}{|1-r_1^j r_2^j \mathrm{e}^{2\mathrm{i}k_{z0}d}|^2}\mathrm{e}^{-2|k_{z0}|d}, & (\beta > k_0), \end{cases} \tag{3}$$

where $k_{z0} = \sqrt{k_0^2 - \beta^2}$ is the wave vector along the z direction, β is the surface-parallel wave vector, and k_0 denotes the vacuum wave vector. The cases of $\beta < k_0$ and $\beta > k_0$ represent propagating and evanescent wave contributions, here r_i^j $(i = 1,\ 2,\ j = \mathrm{s},\ \mathrm{p})$ is the Fresnel reflection coefficients for p- or s-polarized waves. Borophene can be treated as a surface current, so the reflection coefficients (r_th) for the p- and s-polarized electromagnetic waves can be derived according to the boundary condition with the solution of Maxwell's equations.[44]

$$r_l^\mathrm{s} = \frac{p_0 - p_\mathrm{m} - \mu_0 c\sigma_{ll}}{p_0 + p_\mathrm{m} + \mu_0 c\sigma_{ll}}, \tag{4}$$

$$r_l^\mathrm{p} = \frac{p_0\varepsilon_\mathrm{s} - p_\mathrm{m} + \mu_0 c\sigma_{ll} p_0 p_\mathrm{m}}{p_0\varepsilon_\mathrm{s} + p_\mathrm{m} + \mu_0 c\sigma_{ll} p_0 p_\mathrm{m}}, \tag{5}$$

where $p_0 = \sqrt{1-(\beta/k_0)^2}$ and $p_\mathrm{m} = \sqrt{\varepsilon_\mathrm{s} - (\beta/k0)^2}$, μ_0 is the permeability, and c is the speed of light in the vacuum. In the

process of near-field heat transfer, the propagation of tunneling evanescent wave dominates. The contribution to evanescent wave tunneling from s-polarized waves is very weak as compared with p-polarized wave. Therefore, we mainly focus on the tunneling in the s-polarized wave in the subsequent calculations.

3. Results and discussion

We first investigated the near-field HTC between two suspended borophene, graphene, and BP sheets as a function of the gap distance for comparison in Fig. 3. The value of HTC is normalized to the far-field limit of radiatively coupled blackbodies ($q_{\rm bb}$) of 6.03 W·m^{-2}·K^{-2}. The electron density of borophene is taken as 3.3×10^{15} cm $^{-2}$,[43] and the electron relaxation time is 10 fs. We take the maximum electron densities of 7.35×10^{13} cm^{-2} for graphene[45] and 1.0×10^{14} cm^{-2} for black phosphorus.[46] It can be clearly found that the HTC of borophene is the highest when the separation is smaller than 100 nm. But the HTC between graphene or BP sheets is merely 13% and 33.48% of the borophene at 10 nm. In detail, the HTC of borophene reaches up to 1386.86 $q_{\rm bb}$ at a distance of 10 nm, which is mainly caused by its high electron density to support the strong near-field heat transfer.

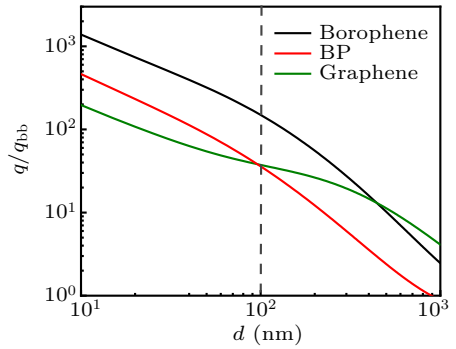


Fig. 3. HTC as a function of gap distance between suspending borophene, BP and graphene sheets.

The influence of different deposited substrates ($\varepsilon_{\rm s}$) on the near-field thermal radiation is presented in Fig. 4. We initially delve into the impact of a lossless substrate on the HTC in Fig. 4(a) with different electron densities of borophene. The HTC is closely related to the dielectric constant of the substrate. It firstly increases to a maximum value and then decreases. At an electron density of $n = 1\times10^{15}$ cm^{-2}, a maximum HTC value of 10.83 kW·m^{-2}·K^{-2} is obtained with a lossless substrate of 4.3. And the peak position of HTC shifts to the left with a smaller n. Figure 4(b) depicts the HTC with different electron relaxation time of borophene. As τ decreases, the peak of the HTC also shifts to the left. Thus, tunable HTC can be obtained with different electron densities. Here we define a switching factor $\eta = 1 - q_{\rm min}/q_{\rm max}$ to represent its tunability. For a substrate with dielectric constant of 4.3, it yields a switching factor of 67.64% when n increases from 1.0×10^{15} cm^{-2} to 3.0×10^{15} cm^{-2}. For a fixed n of 1.0×10^{15} cm^{-2}, the switching factor is 68% when the average electron free time of borophene is increased from 10 fs to 60 fs. Thus, the electron density of borophene shows a significant effect on the HTC, offering a promising way to get tunable HTC.

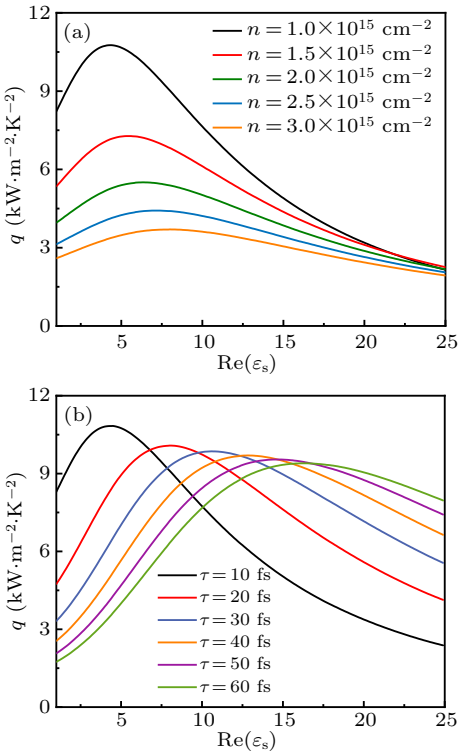


Fig. 4. HTC as a function of lossless substrate (a) with different electron densities of borophene, (b) with different electron relaxation time of borophene.

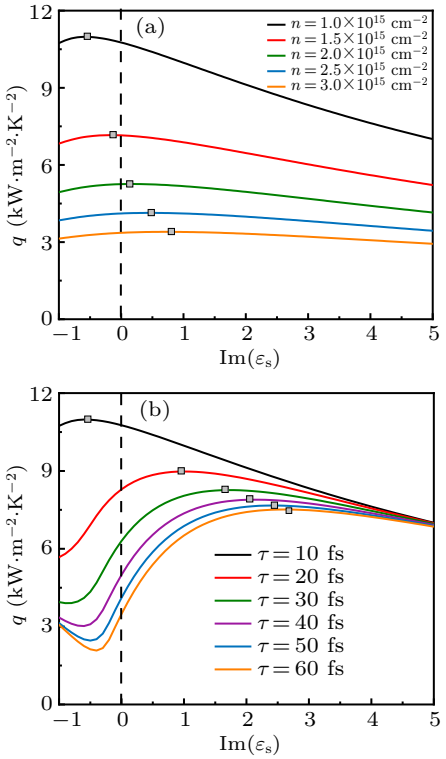


Fig. 5. HTC as a function of lossy substrate (a) with different electron densities of borophene, (b) with different electron relaxation time of borophene.

Now we are in the position to investigate the HTC between two borophene sheets on lossy substrates in Fig. 5. The real part of the dielectric constant is taken as 4.3. Figure 5(a) depicts the HTC on lossy substrates with different electron densities. For a fixed n, the maximum HTC is closely related to the deposited substrate. As the borophene electron density decreases, the peak of the HTC shifts to the left. Figure 5(b) depicts the HTC with different electron relaxation time. As the electron relaxation time of borophene decreases, the trend of the peak of the HTC curve is the same as that of Fig. 5(a).

Figure 6 elaborately explores the influence of the substrate on the HTC. It is found that the peak of HTC shifts to the left as the real part of the dielectric constant increases. Specifically, the imaginary part of the dielectric constant of the substrate undergoes a transition from positive to negative. Then we performed a meticulous calculation of the HTC for the actual value of the substrate around 3.0. It can be found that when Re (ε_s) is larger than 3.14, the lossy substrate will suppress the HTC, when Re (ε_s) is smaller than 3.14, the maximum magnitude of HTC closely depends on the imaginary part of the substrate. The influence of the substrate on the HTC between borophene sheets is further investigated by analyzing the photon tunneling coefficients. We select MoO_3 ($\varepsilon = 4.23 + 0.00024\mathrm{i}$),[47] ZnSe ($\varepsilon = 5.66 + 0.00001\mathrm{i}$)[48] as the substrate, the conventional substrate SiC ($\varepsilon = 10.43 + 0.3238\mathrm{i}$)[49] and the suspended borophene sheet are also included for comparison. Figure 7 displays the contours of ETC along the x and y directions, where the bright areas represent the intensity of the photon tunneling probability. The ETC along the x or y direction varies significantly due to the anisotropic Drude weights,[50] which are used to model the behavior of electrons in materials where the electrons have different mobilities along different directions. The bright branch of BP on the MoO_3 substrate occupies a broader wave vector range in Figs. 7(b) and 7(f) compared to the other three cases. The ETC along the x and y axes splits into two resonance branches between suspended borophene sheets, namely the antisymmetry mode of the wavelet vector and the symmetry mode of the large wave vector in Figs. 7(a) and 7(e). It is due to both the lower and upper vacuum–borophene interfaces supporting evanescent fields that decay exponentially along the direction perpendicular to the interface, allowing the evanescent field of surface plasmon polaritons at one surface to interact with those at the opposite surface.[41] Figures 7(g) and 7(h) show the ETC of borophene sheets on SiC substrate, the bright areas denote the resonance modes of different evanescent waves. The one that appeared at the lower frequency is from the surface plasmon polaritons supported by borophene, while the other at the higher frequency is from the coupling of the surface plasmon polaritons with surface phonon polaritons excited by SiC. It is evident from Fig. 7 that the choice of substrate greatly influences the ETC of borophene sheets. Selecting an appropriate substrate will enhance the photon tunneling probability, thereby increasing the NFRHT between two borophene sheets.

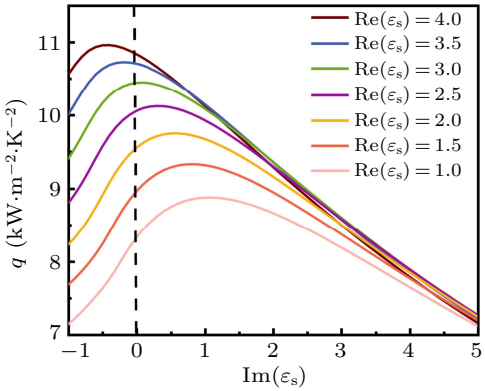


Fig. 6. HTC between borophene sheets on different dielectric substrates.

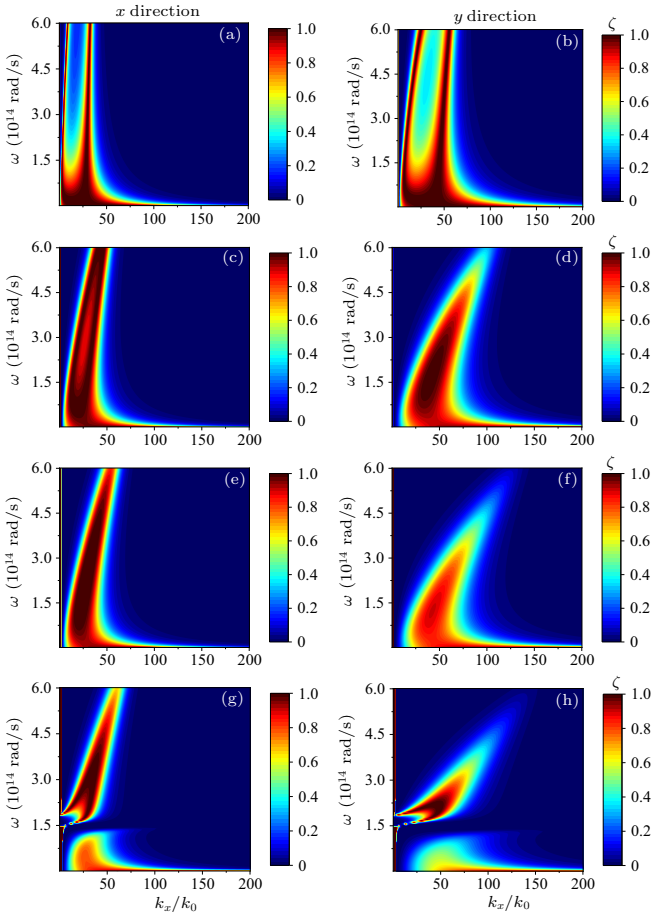


Fig. 7. ETC of borophene sheets on different substrates along x and y directions with a distance of 10 nm: [(a) and (e)] suspended borophene sheets, [(b) and (f)] MoO_3 substrate, [(c) and (g)] ZnSe substrate, [(d) and (h)] SiC substrate.

Finally, the influence of gap distance and temperature of the emitter on the HTC on different substrates are presented in Fig. 8. Due to the tunneling effect of evanescent waves, NFRHT is inversely proportional to the separation distance in Fig. 8(a), the correlation between the HTC and d follows the relation of $q \propto 1/d^2$.[51] In the very near-field ($d \leq 25$ nm),

the HTC between borophene/MoO_3 surpasses that of the suspended borophene sheets and it exceeds the blackbody limit by four orders of magnitudes at the gap of 10 nm. For comparisons, we also selected ZnSe, hexagonal boron nitride (hBN) ($\varepsilon = 4.49 + 0.0046\mathrm{i}$),[52] and TiO_2 ($\varepsilon = 4.75 + 0.00005\mathrm{i}$)[53] as the substrates for comparisons at 10 nm. The corresponding spectral heat flux is 10436.1 $\mathrm{W{\cdot}m^{-2}{\cdot}K^{-2}}$, 10720.4 $\mathrm{W{\cdot}m^{-2}{\cdot}K^{-2}}$, and 10749.9 $\mathrm{W{\cdot}m^{-2}{\cdot}K^{-2}}$, respectively. Obviously, a larger HTC of 10757.3 $\mathrm{W{\cdot}m^{-2}{\cdot}K^{-2}}$ is achieved when MoO_3 is taken as the substrate. When we select the conventional substrate material SiC, the NFRHT between borophenes is suppressed, which leads to a lower HTC. We have also calculated the HTC for a distance of 10 nm with Si and SiO_2[54] as substrates, yielding results of 9613.69 $\mathrm{W{\cdot}m^{-2}{\cdot}K^{-2}}$ and 6578.38 $\mathrm{W{\cdot}m^{-2}{\cdot}K^{-2}}$, respectively. These results indicate that SiO_2 demonstrates considerable potential as a substrate among the commonly used materials. It is worth to mention that when the distance between two sheets is expanded to 10 μm or more, the spectral heat flux is almost invariant and it is independent of the distance between the objects. Figure 8(b) illustrates the variation of HTC between borophene sheets on various substrates when the temperature (T_1) is different at a distance of 10 nm. Under high temperatures, the HTC for different substrates consistently increases as the temperature rises. Compared to the other three cases, the HTC of borophene on the MoO_3 substrate remains the highest with different temperatures, indicating the selection of the substrate is vital to obtain the enhanced NFRHT.

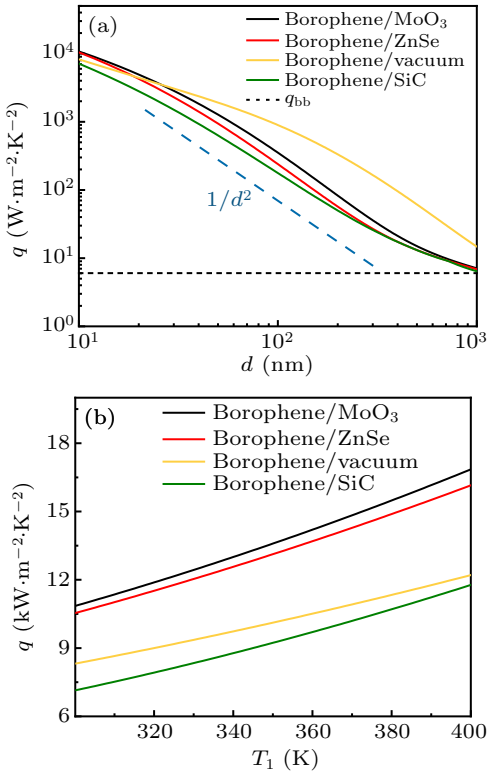


Fig. 8. HTC between borophene sheets on four substrates (a) with different separation d, (b) with different temperatures of T_1.

To carry out the experiment with our proposed design, the possible steps for measuring the HTC between borophene sheets on a substrate are presented. Firstly, a single layer of borophene is synthesized on the metallic substrate by chemical vapor deposition[55] or molecular beam epitaxy, the borophene sheets are then transferred to the target substrate with mechanical stripping.[56] The sample is then placed in a vacuum chamber where the borophene sample is heated to obtain the desired temperature difference. A piezoelectric actuator is taken to adjust the position of the borophene sheets. An interferometric spatial phase imaging system[57] is preferred to precisely measure the gap. Meanwhile, a miniature resistance temperature sensor embedded in the substrate monitors the temperature. Finally, the temperature difference is recorded and a time-dependent heat transfer model is taken to calculate the heat transfer coefficient.[58] In addition, with the rapid development of the nanofabrication technique, further study on the near-field thermal radiation can be initiated between different carbon-based materials.

4. Conclusion

In summary, we have investigated the substrate's influence between two borophene sheets on the NFRHT. Our findings illustrate that the HTC can be effectively modulated by adjusting the electron concentration and relaxation time of borophene. Enhanced HTC between borophene sheets on the dielectric or lossy substrate can be achieved with the finely chosen substrate. In a practical application, borophene sheets deposited on MoO_3, ZnSe, and SiC substrates are considered for comparative analysis. The analysis of ETC indicates that MoO_3 can significantly increase the photon tunneling probability between borophene sheets and thus enhance the NFRHT. This work not only reveals the effect of substrates in thermal management involving borophene but also paves the way for the innovative design of carbon-based thermal devices.

Acknowledgement

Project supported by the Natural Science Foundation of Henan Province, China (Grant No. 232102231023).

References

[1] Huang J P 2020 *Theoretical Thermotics: Transformation Thermotics and Extended Theories for Thermal Metamaterials* (Singapore: Springer)
[2] Zhang Z R, Xu L J, Qu T, Lei M, Lin Z K, Ouyang X P, Jiang J H and Huang J P 2023 *Nat. Rev. Phys.* **5** 218
[3] Xie H L, Yin H Y and Fan C Z 2024 *Chin. Phys. Lett.* **41** 044202
[4] Yang F B, Zhang Z R, Xu L J, Liu Z F, Jin P, Zhuang P F, Lei M, Liu J R, Jiang J H, Ouyang X P, Marchesoni F and Huang J P 2024 *Rev. Mod. Phys.* **96** 015002
[5] Polder D and Van Hove M 1971 *Phys. Rev. B* **4** 3303
[6] Pendry J B 1999 *J. Phys.: Condens. Matter* **11** 6621
[7] Volokitin A I and Persson B N J 2004 *Phys. Rev. B* **69** 045417
[8] Kralik T, Hanzelka P, Zobac M, Musilova V, Fort T and Horak M 2012 *Phys. Rev. Lett.* **109** 224302

[9] van Zwol P J, Thiele S, Berger C, de Heer W A and Chevrier J 2012 *Phys. Rev. Lett.* **109** 264301
[10] Worbes L, Hellmann D and Kittel A 2013 *Phys. Rev. Lett.* **110** 134302
[11] St-Gelais R, Guha B, Zhu L, Fan S and Lipson M 2014 *Nano Lett.* **14** 6971
[12] Song B, Ganjeh Y, Sadat S, Thompson D, Fiorino A, Fernández-Hurtado V, Feist J, Garcia-Vidal F J, Cuevas J C, Reddy P and Meyhofer E 2015 *Nat. Nanotechnol.* **10** 253
[13] Kim K, Song B, Fernández-Hurtado V, Lee W, Jeong W, Cui L, Thompson D, Feist J, Reid M T H, García-Vidal F J, Cuevas J C, Meyhofer E and Reddy P 2015 *Nature* **528** 387
[14] St-Gelais R, Zhu L, Fan S and Lipson M 2016 *Nat. Nanotechnol.* **11** 515
[15] Bernardi M P, Milovich D and Francoeur M 2016 *Nat. Commun.* **7** 12900
[16] Hargreaves C M 1969 *Phys. Lett. A* **30** 491
[17] Hu L, Narayanaswamy A, Chen X and Chen G 2008 *Appl. Phys. Lett.* **92** 133106
[18] Song J L, Cheng Q, Zhang B, Lu L, Zhou X P, Luo Z X and Hu R 2021 *Rep. Prog. Phys.* **84** 036501
[19] Fiorino A, Zhu L, Thompson D, Mittapally R, Reddy P and Meyhofer E 2018 *Nat. Nanotechnol.* **13** 806
[20] Inoue T, Ikeda K, Song B, Suzuki T, Ishino K, Asano T and Noda S 2021 *ACS Photon.* **8** 2466
[21] Li J Y, Gao Y and Huang J P 2010 *J. Appl. Phys.* **108** 074504
[22] Gu W, Tang G H and Tao W Q 2015 *Int. J. Heat Mass Transfer* **82** 429
[23] Shen X, Li Y, Jiang C and Huang J 2016 *Phys. Rev. Lett.* **117** 055501
[24] Ben-Abdallah P and Biehs S A 2014 *Phys. Rev. Lett.* **112** 044301
[25] Fan C Z, Wu C L, Wang Y Y, Wang B and Wang J 2024 *Phys. Rep.* **1077** 1
[26] Yin H Y and Fan C Z 2023 *Chin. Phys. Lett.* **40** 077801
[27] Yin H Y and Fan C Z 2023 *Results Phys.* **45** 106216
[28] Stauber T, Peres N M R and Geim A K 2008 *Phys. Rev. B* **78** 085432
[29] Falkovsky L A 2008 *J. Phys.: Conf. Ser.* **129** 012004
[30] Mikhailov S A and Ziegler K 2007 *Phys. Rev. Lett.* **99** 016803
[31] Mao Y, Zhang H, Xiong J, Liu X P, Wang Q Q and Wang J Q 2024 *J. Phys. D: Appl. Phys.* **57** 255111
[32] Yi X J, Zhong L Y, Wang T B, Liu W X, Zhang D J, Yu T B, Liao Q H and Liu N H 2019 *Eur. Phys. J. B* **92** 217
[33] Zhang Y, Yi H L and Tan H P 2018 *ACS Photon.* **5** 3739
[34] Novoselov K S, Jiang D, Schedin F, Booth T J, Khotkevich V V, Morozov S V and Geim A K 2005 *PNAS* **102** 10451
[35] Song J, Chen L, Jin L, Yao L, Caglayan H and Hu R 2022 *Appl. Phys. Lett.* **121** 171104
[36] Askenazi B, Vasanelli A, Delteil A, Todorov Y, Andreani L C, Beaudoin G, Sagnes I and Sirtori C 2014 *New J. Phys.* **16** 043029
[37] Habibzadeh M, Lin H and Edalatpour S 2023 *J. Quantum Spectrosc. Rad.* **307** 108662
[38] Svetovoy V B, van Zwol P J and Chevrier J 2012 *Phys. Rev. B* **85** 155418
[39] Wang A, Zheng Z and Xuan Y 2016 *J. Quantum Spectrosc. Rad.* **180** 117
[40] Mannix A J, Zhou X F, Kiraly B, Wood J D, Alducin D, Myers B D, Liu X, Fisher B L, Santiago U, Guest J R, Yacaman M J, Ponce A, Oganov A R, Hersam M C and Guisinger N P 2015 *Science* **350** 1513
[41] Zhou C L, Wu X H, Zhang Y and Yi H L 2022 *Int. J. Heat Mass Transfer* **183** 122140
[42] Ling X, Huang S, Hasdeo E H, Liang L, Parkin W M, Tatsumi Y, Nugraha A R T, Puretzky A A, Das P M, Sumpter B G, Geohegan D B, Kong J, Saito R, Drndic M, Meunier V and Dresselhaus M S 2016 *Nano Lett.* **16** 2260
[43] Dereshgi S A, Liu Z and Aydin K 2020 *Opt. Express* **28** 16725
[44] Yi X J, Hong X J, Shehzad K, Wang T B, Xu X M, Liao Q H, Yu T B and Liu N H 2019 *Mater. Res. Express* **6** 025906
[45] Messina R, Ben-Abdallah P, Guizal B and Antezza M 2017 *Phys. Rev. B* **96** 045402
[46] Efetov D K and Kim P 2010 *Phys. Rev. Lett.* **105** 256805
[47] Lajaunie L, Boucher F, Dessapt R and Moreau P 2013 *Phys. Rev. B* **88** 115141
[48] Amotchkina T, Trubetskov M, Hahner D and Pervak V 2020 *Appl. Opt.* **59** A40
[49] Zhang J, Yang B, Yu K, Zhang K, Liu H and Wu X 2023 *Phys. Scr.* **98** 075516
[50] Singh D K and Majumdar P 2018 *Phys. Rev. B* **98** 195130
[51] Pascale M, Giteau M and Papadakis G T 2023 *Appl. Phys. Lett.* **122** 100501
[52] Grudinin D V, Ermolaev G A, Baranov D G, Toksumakov A N, Voronin K V, Slavich A S, Vyshnevyy A A, Mazitov A B, Kruglov I A, Ghazaryan D A, Arsenin A V, Novoselov K S and Volkov V S 2023 *Mater. Horiz.* **10** 2427
[53] Sarkar S, Gupta V, Kumar M, Schubert J, Probst P T, Joseph J and König T A F 2019 *ACS Appl. Mater. Interfaces* **11** 13752
[54] He M Y, Wang Q, Zhang H, Xiong J, Liu X P and Wang J Q 2024 *Phys. Scr.* **99** 035506
[55] Tian S, Wang J Q, Sun S, He M Y, Mao Y, Gao Y and Ding P 2023 *Results Phys.* **49** 106485
[56] Zhang Z, Penev E S and Yakobson B I 2017 *Chem. Soc. Rev.* **46** 6746
[57] Salihoglu H, Nam W, Traverso L, Segovia M, Venuthurumilli P K, Liu W, Wei Y, Li W and Xu X 2020 *Nano Lett.* **20** 6091
[58] Loomis J J and Maris H J 1994 *Phys. Rev. B* **50** 18517